Bull. Mater. Sci., Vol. 31, No. 4, August 2008, pp. 635–638. © Indian Academy of Sciences.

Dielectrical and structural characterization of iron oxide added to hydroxyapatite

C C SILVA*, F P FILHO, M F P GRAÇA, M A VALENTE and A S B SOMBRA
Physics Department, Aveiro University, Aveiro, Portugal

MS received 10 July 2007; revised 19 May 2008

Abstract. In this work we report preparation, structural and dielectric analyses of iron oxide added in hydroxyapatite bioceramic ($Ca_{10}(PO_4)_6(OH)_2$ – HAP). Hydroxyapatite is the main mineral constituent of teeth and bones with excellent biocompatibility with hard and muscle tissues. The samples were prepared through a calcination procedure associated with dry high-energy ball milling process with different iron concentrations (1, 2·5 and 5 wt%). The dielectric analyses were made measuring the sample impedance in the frequency range 1 kHz–10 MHz, at room temperature. The relative permittivity of the ceramics, at 10 MHz, are between 7·13 ± 0·07 (1 wt%) and 6·20 ± 0·11 (5 wt%) while ε'' are between 0·0795 ± 0·008 (1 wt%) and 0·067 ± 0·012 (5 wt%). These characteristics were related to the sample microstructures studied by X-ray diffraction and SEM.

Keywords. Hydroxyapatite; dielectrical analysis; iron oxide.

1. Introduction

It is difficult to imagine the present medicine without the possibility of reconstruction of parts of the human body with implants (Vogel and Höland 1987; Hench 1993; Pajamäki *et al* 1995). The first materials used for implants frequently caused inflammations and rejections. For the use in medicine the materials must not have a significant influence in the metabolism. Several materials and composites are used in the production of prosthesis, for example, metallic alloys, metallic materials with hydroxyapatite film, alumina and polyethylene (Zeng and Lancefield 2000). The hydroxyapatite (HAP) is used in orthopedics surgeries (Sugimoto *et al* 1996) and odontological for wadding or surfaces covering, this despite its weak mechanical properties (Weeber and Bakker 1988). To improve the mechanical properties of hydroxyapatite several studies present the substitution of calcium, in the HAP structure, by metals (Elliot 1994) or ions as for instance, silicon and magnesium (Kim *et al* 2003), lead (Xiu *et al* 2004), titanium and zirconium (Silva *et al* 2004) and alumina (Viswanath and Ravishankar 2006). The presence of iron in the apatite structure seems to be important because iron is a vital element in the circulatory system and is essential for the functioning of numerous proteins in cells (Morrissey *et al* 2005). Biomaterials with iron have a very important role in medicine, for example, ferrimagnetics bioglass ceramics (FBC) was introduced for hyperthermic treatment of bone cancer (Kokubo *et al* 1992; Leventouri *et al* 2005). They are complex, multiphase, biocompatible and bioactive materials, motivating us to dope the hydroxyapatite with that metal. The main aim of this work is to determine how iron oxide is introduced into the apatite structure. Structural, optical, electrical, dielectric and magnetic measurements will be done to characterize such bioceramics.

This paper reports the preliminary results of the relative permittivity behaviour vs structure modifications, due to the addition of iron oxide to hydroxyapatite. The dielectric properties of HAP are of interest because electromagnetic fields have been shown to accelerate healing in bone fractures. In addition, an interest in the dielectric properties of HAP stems from the suggestion that electrically insulating HAP coatings might be used on implantable devices (Timothy and Eldon 2002; Silva *et al* 2005).

2. Experimental

The HAP crystalline powders were prepared by a high-energy dry milling, for 20 h. The chemical equation (1) represents the expected chemical reaction:

$$6CaHPO_4 + 4Ca(OH)_2 \rightarrow Ca_{10}(PO_4)_6(OH)_2 + 6H_2O. \quad (1)$$

For the reaction, the starting materials ($CaHPO_4$ and $Ca(OH)_2$), with stoichiometric proportionality for 10 g of total powder, were placed in a stainless steel vessel inside a Fritsch Pulverisette 6 planetary mill system. The ratio between powders and ball mass was near 1/6. The reaction was performed using 370 rpm for 20 h in air. To avoid excessive heat the milling was performed in 60 min milling steps with 10 min pauses.

*Author for correspondence (ccsilva@ua.pt)

Different weight percentages of iron oxide (Fe_2O_3) (1, 2·5 and 5%) were added to the obtained powder. After this the obtained HAP with iron oxide powder added were submitted to a calcination process at 1150°C for 24 h with a heating rate of 4°C/min.

The X-ray diffraction (XRD) patterns were obtained at room temperature using powder samples in an X'Pert MPD Philips diffractometer (with K_α radiation, λ = 1·54056 Å) at 40 kV and 30 mA. Intensity data were collected by the step counting method (step 0·02° and a time per step of 1s) between 20 and 60° (2θ). The output data obtained from Rietveld (1967) refinement was used to calculate the crystallite size. The analysis of the crystallite size (L_c) of the HAP and $Ca_2Fe_2O_5$ phases has been done for all samples using the Scherrer's equation (Azároff 1968):

$$L_c = \frac{k\lambda}{\beta \cos\theta}, \tag{2}$$

where k is the shape coefficient (k = 1 was chosen, considering that the shape of this point is spherical), λ the wavelength, β the full width at half maximum (FWHM) of the peak of each phase and θ the diffraction angle. For this purpose, we chose the single peak near 25·8 (2θ degree) within the pattern and according to $P6_3/m$ space group of HAP whose peak corresponds to hkl = 002 and 33·4 (2θ degree) within the pattern and according to $Pnma$ space group of $Ca_2Fe_2O_5$. This peak corresponded to hkl = 141, both along the c crystallographic axis. We have used the LaB_6 (SRM 660 – National Institute of Standard Technology) powder standard pattern to determine the instrumental width (w_{inst} = 0·087°) and afterwards to calculate the crystallite size via (2). The β parameter has to be corrected using the following equation:

$$\beta = \sqrt{w_{exp}^2 - w_{inst}^2}, \tag{3}$$

where w_{exp} and w_{inst} are the experimental and instrumental width, respectively. w_{inst} was obtained from LaB_6 powder standard pattern using the following expression:

$$w_{inst} = \sqrt{Utg^2\theta + Vtg\theta + W}, \tag{4}$$

where U, V and W were obtained from the output file extracted from Rietveld refinement parameters of LaB_6 samples (Rietveld 1967). The morphological analysis of the sample structure was performed using the scanning electron microscopy (SEM), Philips XL-30, operating with bunches of primary electrons ranging from 12 to 20 keV.

For the dielectric measurements, the samples were prepared from the powders as discs of $1{\cdot}2 \times 10^{-2}$ m diameter for all samples, with an average thickness of 1·85 mm for 5 wt%, 2·39 mm for 2·5 wt% and 3·23 mm for 1 wt%. The pellets were sintered at 900°C for 5 h with the purpose of achieving a compact sample. The electrodes were formed by painting with silver paste (Joint Metal-PC200) on the opposite sides of the samples.

The dielectric data was carried out with a HP 4291A Material Impedance Analyzer in conjunction with a HP 4194 Impedance Analyzer, which jointly covered the frequency region from 1 kHz to 40 MHz, at room temperature (300 K), measuring the sample capacitance and dielectric loss.

3. Results and discussion

Figure 1 presents the XRD pattern of the reaction of hydroxyapatite added with iron oxide at different weight

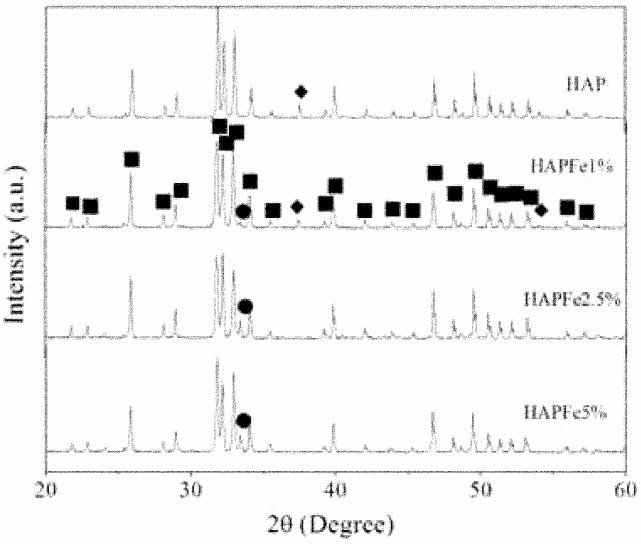

Figure 1. XRD patterns of the HAP, HAPFe1%, HAPFe2·5% and HAPFe5% samples. HAP (■), $Ca_2Fe_2O_5$ (●) and CaO (◆) (JCPDS–Pattern 74-0566, 47-1744 and 77-2376).

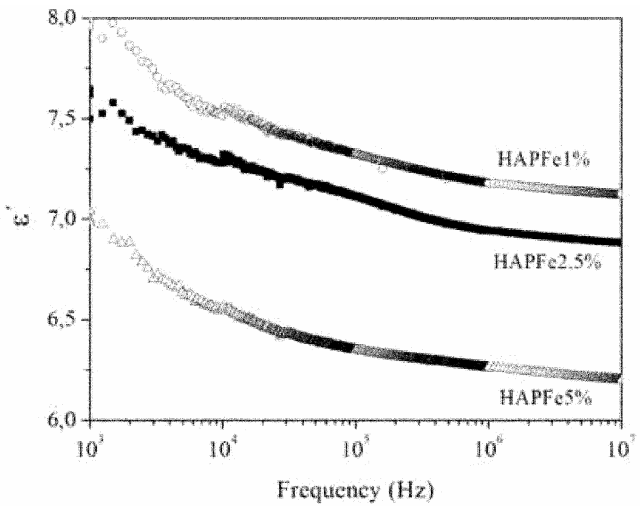

Figure 2. ε' vs frequency at 300 K for all the samples.

Table 1. Measure of the relative permittivity for the samples at 10 MHz (300 K) and crystalline size [HAP (μm) and $Ca_2Fe_2O_5$ (nm)].

Sample	HAPFe1%	HAPFe2·5%	HAPFe5%	HAP [19–20]
ε′	7·13 ± 0·07	6·88 ± 0·09	6·20 ± 0·11	11·09
ε″	0·0795 ± 0·0008	0·0819 ± 0·0011	0·0670 ± 0·0012	–
$Ca_2Fe_2O_5$ (nm)	49·9 ± 3·2	67·5 ± 5·6	95·9 ± 9·5	–
HAP (μm)	0·20 ± 0·014	0·77 ± 0·018	0·81 ± 0·018	0·02 ± 0·54

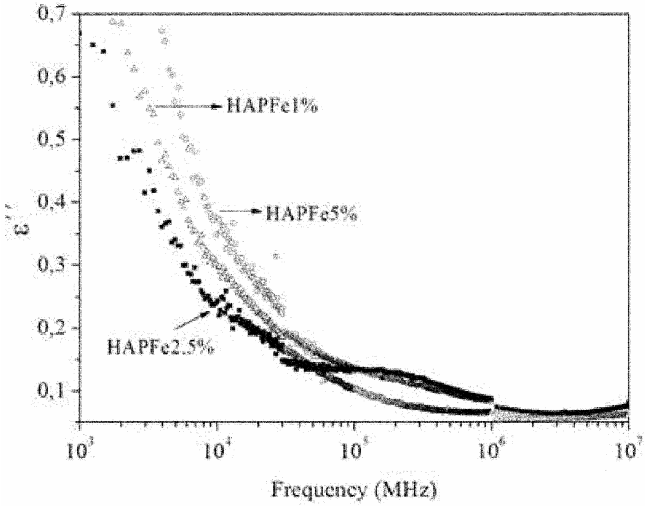

Figure 3. ε″ vs frequency at 300 K for all the samples.

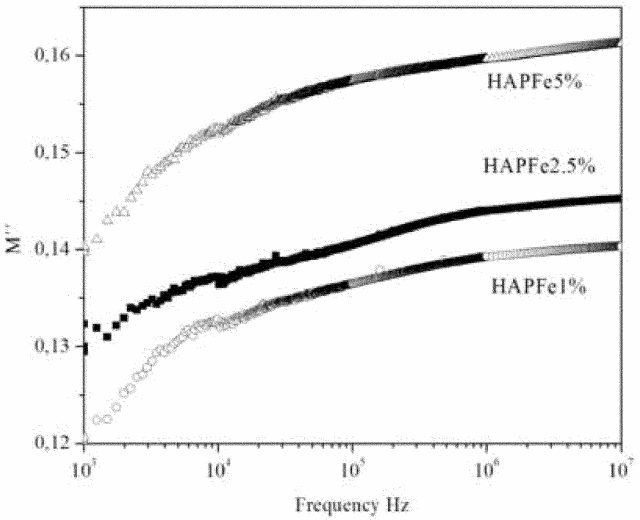

Figure 4. *M*″ vs frequency at 300 K for all the samples.

percentages (1, 2·5 and 5%). It is identified as the hydroxyapatite phase (JCPDS) and iron brownmillerite ($Ca_2Fe_2O_5$) (JCPDS) in all samples. The formation of the brownmillerite indicates that the added iron oxide was inserted into the $Ca_2Fe_2O_5$ phase. This phase increases with iron concentration showing calcium–iron interaction. Other identified phase was CaO, formed through the dissociation of the $Ca(OH)_2$ (JCPDS) during the calcination process. This phase is present in the HAP before the addition of the iron oxide (figure 1) and it disappears in the 2·5% wt sample.

The relative permittivity (ε') vs frequency (figure 2) decreases with the rise of the concentration of iron oxide and with increasing frequency for all the studied samples (table 1).

Figure 3 shows the frequency dependence of ε'', out of phase parts of the dielectric permittivity. In the graph of figure 3 the value of frequency starts at 10^3 Hz because at lower frequencies the scattering of ε'' values is very large. At 10 MHz, the ε'' values are between 0·0795 ± 0·0008 (1 wt%) and 0·067 ± 0·0012 (5 wt%), and also decrease softly with the rise of the added iron oxide concentration to hydroxyapatite (figure 3 and table 1). A similar behaviour was observed in all other measured frequencies. The values obtained at 10 MHz for the ε' and ε'' are shown in table 1.

Analysing the ε^* frequency dependence (figures 2 and 3), it suggests that in this frequency range these samples do not have relaxation mechanisms.

Figure 4 shows the frequency dependence of the imaginary part of M^* ($M^* = (\varepsilon^*)^{-1} = 1/(\varepsilon' - j\varepsilon'')$ (Silva *et al* 2005)). This formalism, which minimizes the electro sample interface capacitance contribution at low frequencies, emphasizes small features at low frequencies, revealing that these samples do not present relaxation mechanisms in this frequency range.

From the XRD pattern analysis (2), it was observed that the samples HAPFe1%, HAPFe2·5% and HAPFe5% have $Ca_2Fe_2O_5$ crystallites with sizes of ~49·9 ± 3·2, 67·5 ± 5·6 and 95·9 ± 9·5 nm (table 1), respectively and hydroxyapatite (HAP) crystallites with ~0·20 ± 0·014, 0·77 ± 0·018 and 0·81 ± 0·018 μm (table 1).

The SEM micrographs show particles having larger dimensions than those calculated by XRD (figures 5a and b) suggesting the existence of agglomerates of crystallites. Nevertheless, both XRD and SEM results reveal that the crystallites and particle sizes increase with the rise of the iron oxide concentration. The undoped hydroxyapatite, in the ceramic form, presents a $\varepsilon' \sim 11{\cdot}09$ (table 1) with crystallite size of ~20·63 ± 0·54 nm (Silva *et al* 2005, 2006). The HAP-Fe microscopic results (figure 5) show images with a strong variation of the microstructure with iron oxide concentration. Spherical particles dispersed in the form of grain duplex (figure 5a) are observed through back scattering electron (BSE) method in the sample with the lowest percentage of added iron oxide (1%) assigned to

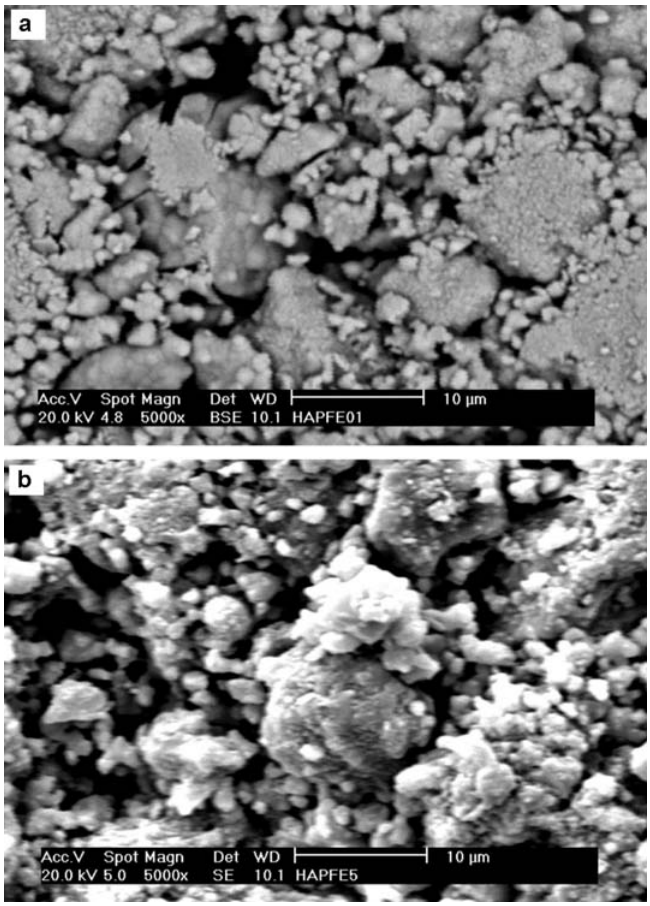

Figure 5. SEM micrographs of the sample: **a**. HAP-Fe 1% with 5000X and **b**. HAP-Fe 5% with 5000X.

a long time of calcinations and sinterization. Thus, the increase of the crystalline size of HAP phase should lead to a more uniform microstructure (figure 5).

By comparing the dielectric results of these samples with those of the bare HAP, it is observed that the incorporation of iron oxide in the brownmillerite ($Ca_2Fe_2O_5$) phase and the increase of the crystallites sizes of HAP and ($Ca_2Fe_2O_5$), due by the calcination and sinterization time are the main effects responsible for the observed decrease of ε' and ε'' (table 1).

4. Conclusions

$Ca_2Fe_2O_5$ (brownmillerite) phase was obtained with the addition of iron oxide to hydroxyapatite samples. The formation of the brownmillerite indicates that the iron oxide has reacted with the HAP during the sintering process. This phase increases with the iron concentration showing calcium–iron interaction. The real part of the relative permittivity (ε') and the out of phase part of the relative permittivity (ε''), decrease from the sample with 1% of iron oxide to the sample with 5%. The decrease of the ε' can be ascribed to the rise of crystalline size of HAP phase and to the $Ca_2Fe_2O_5$ phase. The particles size of HAP and $Ca_2Fe_2O_5$ phases in the sintered samples increases with the rise of Fe_2O_3 concentration.

Acknowledgements

The authors thank the Physics Department (I3N), Aveiro University, LOCEM (Physics Department, Federal University of Ceará, Brazil) for the use of their laboratories for samples preparation and Fundação para a Ciência e Tecnologia (FCT) for financial support (SFRH/BPD/26715/2006).

References

Azároff L V 1968 *Elements of X-ray crystallography* (McGraw-Hill Book Company)

Elliott J C 1994 *Structure and chemistry of the apatites and other calcium orthophosphates*, in *Studies in inorganic chemistry* (Amsterdam, The Netherlands: Elsevier Science and Technology) **18** p. 137

Hench L L 1993 *Introduction*, in *An introduction to bioceramics* (eds) L L Hench and J Wilson (New Jersey, USA: World Scientific) **1** pp 1–24

Ikenaga M, Ohura H, Nakamura T, Kotoura Y, Yamamuro T, Oka M, Ebisawa Y and Kokubo T 1991 *Bioceramics* **4** 255

JCPDS–Pattern 74-0566 (HAP-REF), 47-1744 ($Ca_2Fe_2O_5$), 77-2376 (CaO)

Kim S R, Lee J H, Kim Y T, Riu D H, Jung S J, Lee Y J, Chung S C and Kim Y H 2003 *Biomaterials* **24** 1389

Kokubo T, Ebisawa Y, Sugimoto Y, Kihiama M, Ohura K, Yamamuro T, Hiraoka M and Abe M 1992 *Bioceramics* **5** 213

Leventouri Th, Kis A C, Thompson J R and Anderson I M 2005 *Biomaterials* **26** 4924

Morrissey R, Rodríguez-Lorenzo L M and Gross K A 2005 *J. Mater. Sci.: Mater. Med.* **16** 387

Ohura K, Ikenaga M, Takashi N, Yakao Y, Yukihiro E, Tadashi K, Yoshihiro K and Masanori O 1991 *J. Appl. Biomater.* **2** 153

Pajamäki K J J , Lindholm T S, Andersson Ö H, Karlsson K H, Vedel E, Yli-Urpo A and Happonen R P 1995 *J. Mater. Sci.: Mater. Med.* **6** 14

Rietveld H M 1967 *Acta Crystallogr.* **22** 151

Silva C C, Valente M A, Graça M P F and Sombra A S B 2004 *Solid State Sci.* **6** 1365

Silva C C, Valente M A, Graça M P F and Sombra A S B 2005 *Non-crystalline Solids* **351** 2945

Silva C C, Valente M A, Graça M P F and Sombra A S B 2006 *Non-crystalline Solids* **352** 1490

Sugimoto T, Dirige G E and Maramatsu A 1996 *J. Colloid & Interf. Sci.* **182** 444

Timothy P H and Eldon D C 2002 *J. Biomed. Mater. Res. Part A* **60** 643

Viswanath B and Ravishankar N 2006 *Scr. Mater.* **55** 863

Vogel W and Höland W 1987 *Angew. Chem. Int.* **26** 527

Weeber A W and Bakker H 1988 *Physica* **B153** 93

Xiu Z, Mengkai L, Feng G, Shufen W, Dong X and Duorong Y 2004 *Inorg. Chem. Commun.* **7** 604

Zeng H and Lancefield W R 2000 *Biomaterials* **21** 23